Potential and limitations of space-based methods for the retrieval of surface UV-B daily doses: A numerical study

L. Bugliaro,[1] B. Mayer,[1] R. Meerkötter,[1] and J. Verdebout[2]

Received 26 July 2005; revised 27 December 2005; accepted 19 April 2006; published 12 December 2006.

[1] For a typical space-borne algorithm for the estimation of surface UV-B daily doses, the implications of a limited temporal sampling of cloud properties and of the neglect of three-dimensional radiative effects are addressed. By means of six synthetic diurnal cloud cycles, different temporal samplings of cloud properties have been investigated, while surface and atmospheric properties have been kept constant. The results have been compared with benchmark calculations of the daily doses using a 15 min time step. The neglect of the horizontal photon transport imposes limitations to the estimation of daily doses since it leads to statistical uncertainties up to 25% and biases ranging from 3% to 9%. Additionally, when a reduced temporal sampling is used, maximum uncertainties increase up to 85% when probing the cloud field only every 4 hours. Even in this case, however, 25–40% of the daily doses in the model domain have an accuracy between −20% and +20%. The time around noon turns out to be of crucial importance for a precise estimation of UV daily doses. Therefore usually a limited number of cloud probes around noon is particularly efficient, although in case of high temporal and spatial cloud variability throughout the day three cloud probes can still be too few to prevent the occurrence of large (>80%) deviations. Finally, by spatial averaging, a large improvement of the agreement between reference values and daily doses computed with a given time sampling can be achieved.

Citation: Bugliaro, L., B. Mayer, R. Meerkötter, and J. Verdebout (2006), Potential and limitations of space-based methods for the retrieval of surface UV-B daily doses: A numerical study, *J. Geophys. Res.*, *111*, D23207, doi:10.1029/2005JD006534.

1. Introduction

[2] Surface ultraviolet (UV) radiation has become a key issue since the decrease of total ozone was observed for the first time in the early 1980s at middle and high latitudes. UV radiation can have detrimental effects not only on human health but also on aquatic and terrestrial ecosystems and on materials. Even if the fundamental aspects of UV radiative transfer are well understood, the need for monitoring surface UV is still great. Satellite-based algorithms find here a very important and useful application because they represent powerful tools for investigating the impact of UV radiation over wide areas, thus offering a much better spatial coverage than surface instruments. However, methods based on satellite data can only operate indirectly through the determination of the main quantities affecting surface UV radiation. Besides ozone, these are clouds, aerosol, altitude, and surface albedo, in particular in the presence of snow or ice. Except for altitude, their determination is still limited by spatial and/or temporal resolution given by the intrinsic characteristics of satellite orbits and instruments. This is especially true since great interest lies in the determination of daily doses of surface UV radiation, which implies that the diurnal cycles of all UV affecting parameters should be accounted for. However, this is a challenge in particular for clouds, which are known to be highly variable during the day. Nevertheless, their determination is essential since they represent the main modulation factor for UV.

[3] Several independent methods have been developed for the mapping of surface UV by exploitation of various instruments aboard different satellites [*Eck et al.*, 1995; *Lubin and Jensen*, 1995; *Meerkötter et al.*, 1997; *Lubin et al.*, 1998; *Krotkov et al.*, 1998, 2001; *Peeters et al.*, 1998; *Herman et al.*, 1999; *Verdebout*, 2000; *Verdebout and Vogt*, 2002; *Slaper et al.*, 2001; *Wuttke et al.*, 2003]. All of those make some common assumptions: First, they neglect three-dimensional (3-D) radiative effects using the independent pixel approximation (IPA) [see *Nack and Green*, 1974; *Bodeker and McKenzie*, 1996; *Scheirer and Macke*, 2001]. Second, time resolution is usually limited either by the availability of satellite data (polar orbiting systems) or by CPU processing time and disk space. In consequence, the daily cycle of clouds is only partially taken into account. Both aspects lead to errors in the determination of daily

[1]Institute for Atmospheric Physics, Deutsches Zentrum für Luft- und Raumfahrt, DLR Oberpfaffenhofen, Germany.
[2]Institute for Health and Consumer Protection, European Commission-Joint Research Centre, Ispra, Italy.

0148-0227/06/2005JD006534

doses of ultraviolet surface radiation. The diurnal cycle of other UV affecting parameters (like ozone) is less pronounced and plays a minor role.

[4] *Kalliskota et al.* [2000] and *Arola et al.* [2002] have already presented studies about the accuracy of satellite derived daily doses by comparing them to surface measurements. *Martin et al.* [2000] have addressed the problem from a more theoretical point of view. They investigated the accuracy of one-dimensional (1-D) erythemal daily doses from one noontime determination of the cloud optical depth by means of a method "mimicking a 'perfect' satellite algorithm." They compared them with surface UV measurements at two Alpine sites in Europe and found that the root-mean-square (rms) difference is about 20%. In our numerical study, based on a set of synthetical diurnal cloud cycles, we are able to separately address the above two approximations (IPA versus 3-D radiative transfer and time sampling of clouds). Uncertainties in the input parameters (due to limitations of the retrieval methods or the lacking knowledge about the actual state of the atmosphere) as well as other error sources that may be present in the satellite-based algorithm can be excluded through our approach [*Krotkov et al.*, 1998; *Herman et al.*, 1999; *McKenzie et al.*, 2001].

[5] Some of these aspects, which are essential for the estimation of daily doses, are of little concern when computing monthly doses. In the latter case, many of the errors present in the daily doses cancel out so that even with one noontime cloud probe very good results (accuracy better than 10%) can be achieved [see *Martin et al.*, 2000; *Lubin et al.*, 1998; *Arola et al.*, 2002].

[6] Section 2 is concerned with model input. Section 2.1 presents the illumination conditions chosen, section 2.2 introduces six different diurnal cloud cycles, and in section 2.3 the radiative transfer model is described. In sections 3.1–3.4 we define three time sampling schedules and in section 3.5 some important aspects related to radiative transfer are exposed that will be needed for a detailed understanding of the results. These are illustrated in sections 4 and 5. The former deals with the uncertainty introduced in the calculation of satellite-based daily doses by the use of the IPA approximation for radiative transfer. Hereafter (section 5), the limited temporal sampling of a space-borne instrument is also taken into account and the accuracy of the resulting daily doses is evaluated. The effect of spatial averages is addressed in both sections 4 and 5. Finally, section 6 presents summary and conclusions.

2. Model Input

[7] The diurnal cycles of clouds and solar zenith angle are of central importance for the simulation of UV daily doses. Both topics are addressed in the first two subsections (2.1 and 2.2). Section 2.3 deals with the radiative transfer model and its input parameters.

2.1. Location and Time

[8] Surface UV daily doses are computed for different diurnal cycles of clouds for two distinct sets of diurnal courses of solar zenith angles as shown in Figure 1. Here CET stands for Central European Time (UTC+1). The first curve, although rather flat (minimum solar zenith angle 68.07° at 1212 CET), describes a spring day with a relatively long illumination time of almost 12 hours (sunrise at 0612:30 CET, sunset at 1811:11 CET); the second one represents a summer day where the sun rises much higher above the horizon (minimum solar zenith angle 14.55° at 1205 CET) for an overall daytime duration of about 14 hours 40 min (sunrise at 0446:03 CET and sunset at 1924:32 CET).

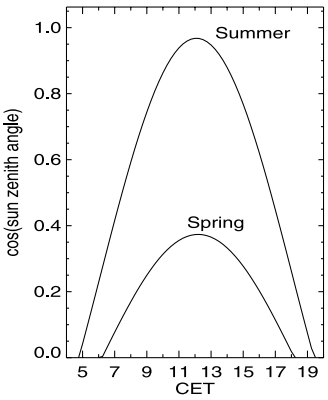

Figure 1. Daily runs of the cosine of the solar zenith angles for a spring day at 68°N 14°E and a summer day at 38°N 14°E.

[9] These two situations (in the following simply referred to as "spring" and "summer") show extreme examples of solar illumination under which the investigation of daily doses is of strong interest. The spring day corresponds to conditions encountered at the beginning of spring (21 March) at the Lofoten Islands (68°N 14°E). This region serves as spawning area for Arctic cod, a species of strong commercial interest that was the object of study of the EC-funded UVAC project in which the authors were involved. The summer day, on the other hand, corresponds to particularly high UV stress conditions encountered in southern Europe (38°N 14°E) at the summer solstice (21 June).

2.2. Diurnal Cloud Cycles

[10] For a model domain of 15 km × 15 km, six series of cloud optical depth distributions are constructed that represent six different synthetic diurnal cloud cycles (called CC1–CC6). Each of them consists of 58 cloud fields and every single cloud field represents a 15 × 15 pixel area according to a real cloud scene as observed by the NOAA/AVHRR instrument. These satellite data have been received at the German Remote Sensing Data Centre (DFD) of the DLR at Oberpfaffenhofen, processed by the APOLLO software package [*Kriebel et al.*, 1989, 2003], and remapped onto a grid with 0.01° resolution in latitude and 0.0125° longitude (approximately 1 × 1 km^2) ranging from 34°N to 72°N in latitude and from −11°E to 32°E in longitude. We use the horizontal distribution of vertically integrated cloud optical thicknesses.

[11] Each diurnal cloud cycle stems from a single AVHRR scene where the spatial displacement of a 15 × 15 pixel area along a fixed latitude simulates the temporal evolution of clouds. For all cloud cycles CC1 to CC6 the time 0500 CET is assigned to the first area in the series while the time delay between successive areas is fixed to

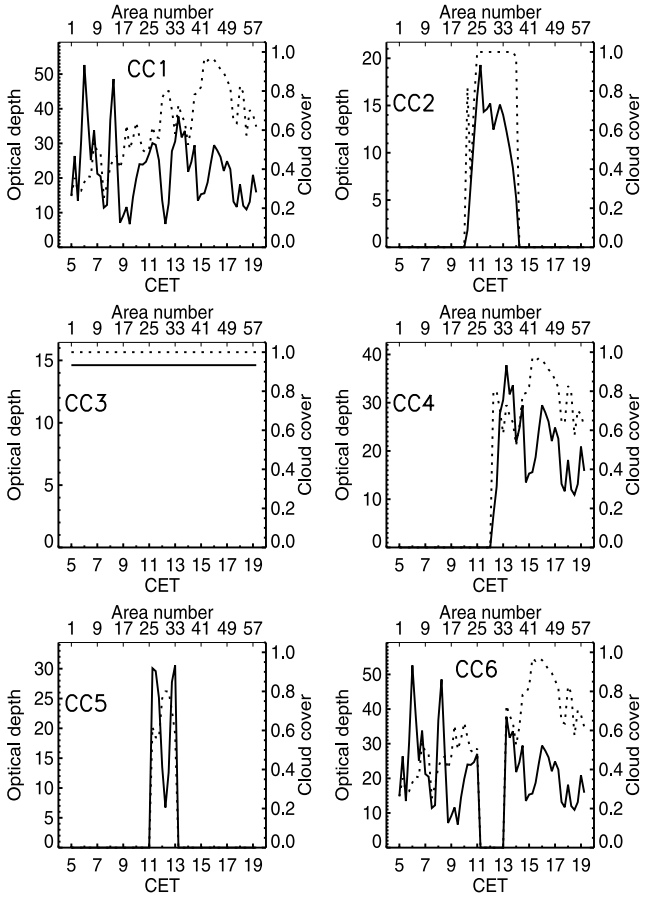

Figure 2. Daily cycles of cloud cover (dotted line) and mean optical depth of the cloudy pixels (solid line) as a function of time and area number.

15 min. The last area, area number $n = 58$, thus corresponds to time 1915 CET. In this manner, a diurnal cycle of cloud fields is obtained that covers the time between sunrise and sunset in the summer day. To simulate the spring day, the subset representing the time interval 0615–1800 CET is extracted from CC1 to CC6, respectively, which means area 6 to area 53 for an overall number of 48 areas. The cloud cycles for the spring day and the summer day coincide at noon.

[12] Each diurnal cloud cycle is characterized as follows (see Figure 2):

[13] 1. For the first cloud cycle the NOAA-14 overpass at 1305 UTC on 15.03.1997 is chosen. The northern part of this scene (Figure 3, left) was selected to get broken cloud conditions.

[14] 2. The second cloud cycle stems from the center part of the NOAA-14 overpass at 1304 UTC on 15.06.1997 (Figure 3, right) to produce a systematic difference in cloud cover between the time around noon and the rest of the day. The first 21 and the last 21 appointed times are cloud-free, while areas corresponding to times around noon are overcast.

[15] 3. The third cloud cycle represents a fully cloudy situation with a cloud field that remains constant all over the day, using area 28 of CC2 for all time steps. Its spatial distribution of optical depths is not homogeneous but has a rms deviation of approximately 3.5 around the mean value of 14.6.

[16] 4. The fourth cloud cycle is a combination of cloud-free areas in the morning with a subset of the first cloud cycle in the afternoon: Areas 1 to 29 are cloud-free, while areas 30 to 58 are the same as in CC1 (broken clouds).

[17] 5. The fifth cloud cycle is again a combination of cloud-free areas with a subset of CC1: Areas 1 to 25 and 34 to 58 are cloud-free, while areas 26 to 33 are extracted from CC1. This cloud cycle differs from CC2 in that the cloudy part of the day is shorter and cloud cover is never equal 1.0.

[18] 6. The sixth cloud cycle is the inverse of CC5. Here the areas around noon are cloud-free, while all the others are inherited from CC1.

[19] These synthetical cloud cycles provide realistic but challenging scenarios for every satellite-based algorithm for the computation of UV daily doses. On one side, they represent conditions under which UV radiation is a concern, since cloud cover is not complete and/or cloud optical depth

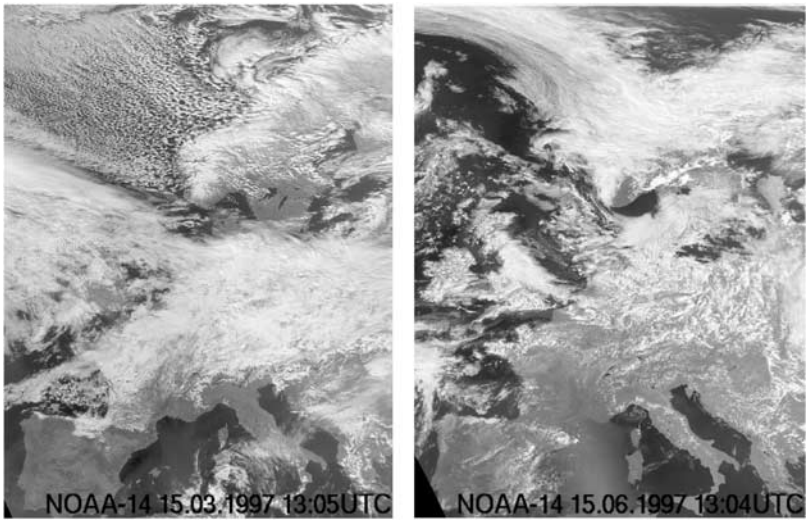

Figure 3. Greyscale composites of subsets of the NOAA/AVHRR overpasses at 1305 UTC on 15.03.1997 (left) and at 1304 UTC on 15.06.1997 (right) used for the generation of the cloud fields.

is not too large. On the other side, it is very difficult for a space-based method to account for their spatial and temporal variability due to the reasons expressed in the introduction. Thus these cases of abrupt variability of cloud field structures can help to determine essential features like upper and lower bounds for the accuracy that can be reached by satellite-based methods in the computation of UV daily doses. In reality, when the temporal variation of clouds over the day is less pronounced, the accuracy reached by satellite-based algorithms is expected to lie between these limits. On the other side, some situations like the evolution of clouds through convection could lead to even greater uncertainties that could not be fully represented in this study.

[20] As input to the radiative transfer model the spatial resolution of the cloud fields extracted from the NOAA/AVHRR scenes is set to 1 km × 1 km. A higher resolution would certainly be desirable, to get a better estimate of cloud structure. The resolution of 1 km, however, seems to be about the optimum choice for cloud optical property retrievals: For higher resolution, net horizontal photon flux starts becoming relevant and the assumption of independent pixels is no longer valid. For lower resolution, the inhomogeneity within a pixel causes the so-called plane-parallel bias [e.g., *Cahalan et al.*, 1994; *Varnai and Marshak*, 2001; *Zinner*, 2004]. Thus at this resolution the geometric features of clouds are reasonably rendered (even if not all 3-D effects can be reproduced) and the cloud optical depths are correctly retrieved.

2.3. Radiative Transfer Model

[21] We apply the radiative transfer model SHDOM (Spherical Harmonics Discrete Ordinate Method) by *Evans* [1998]. This model is run in two modes: a fully three-dimensional (3-D) and an independent pixel approximation (IPA) mode based on a 1-D algorithm relying on the Eddington approximation. The first one includes all relevant three dimensional radiative interaction processes. In the IPA mode the interactions between neighboring pixels are neglected but multiple scattering and absorption processes within each pixel are taken into account. In this way the optical properties can be specified on a common internal spatial grid with 250 m × 250 m horizontal resolution and 77 levels vertical resolution with the top of the atmosphere at 100 km. Each model cloud scene has an area of 15 × 15 km^2 and is subject to periodic boundary conditions in horizontal directions. Owing to the 1 km resolution of the input cloud optical depth distributions, results are eventually averaged from the internal grid resolution to the input grid resolution. The finally 225(= 15 × 15) pixels of 1 km resolution, representing 225 daily doses for each cloud cycle, provide a meaningful statistical ensemble.

[22] Calculations are performed in the UV-B spectral range at 305 nm, which quite well represents the erithemally weighted irradiance. The extraterrestrial solar flux has been adopted from the Atlas 3 [*Kaye and Miller*, 1996] spectrum.

[23] Comparing the 3-D model SHDOM to surface measurements for cloudless conditions *Degünther et al.* [1998] found that for wavelengths below 320 nm the deviations do not exceed 10%. The Intercomparison of 3-D Radiation Codes [*Cahalan et al.*, 2005] was a detailed comparison of 3-D models with each other, while Figure 4 shows the accuracy of the IPA mode with respect to the 3-D mode. Shown are relative differences between 3-D and IPA dose rates as a function of cloud optical depth and solar zenith angle for 1-D plane-parallel clouds. The largest deviations of 5 to 9% occur for a solar zenith angle of 80°, where the absolute values of UV dose rates are very small compared to the noon values. Since large solar angles contribute only little to UV daily doses, relative differences of UV daily doses should not exceed 2–3% in summer and 4–5% in spring, when the horizontal inhomogeneity of cloud structures can be neglected. Deviations have to be ascribed to the different model approaches and to the fact that SHDOM, unlike Monte Carlo models, represents an approximation of the (3-D) radiative transfer equation.

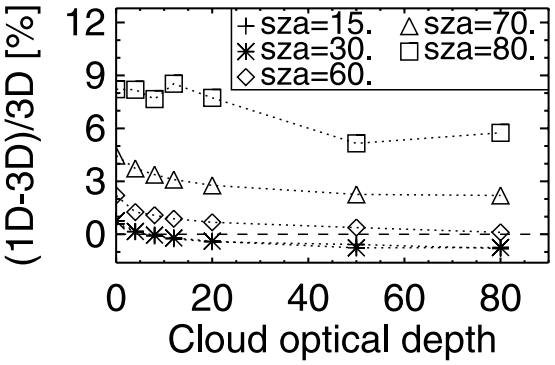

Figure 4. Relative differences between three-dimensional (3-D) and IPA dose rates as a function of cloud optical depth and solar zenith angle (sza) at a wavelength of 305 nm.

[24] The 3-D mode allows to simulate surface UV radiation as realistic as possible, while IPA is usually employed for the calculation of UV maps (see section 1). Typical three-dimensional effects are for instance the shadow displacement due to the relative geometric position of sun and clouds, the contribution of remote clouds to the UV radiation (as explained by *Degünther and Meerkötter* [2000]), or the enhancement of surface UV levels above the clear-sky values in case of broken clouds when the direct sun beam is not blocked [*Bodeker and McKenzie*, 1996; *Mims and Frederick*, 1994]. This increased surface UV radiation is caused by reflection at cloud edges or by scattering between the ground and the cloud base [*Meerkötter and Degünther*, 2001]. These effects, all inherent in the 3-D nature of atmospheric radiative transfer, cannot be taken into account by the IPA and represent principle limitations of 1-D radiative transport schemes and of all algorithms based on them.

[25] The Subarctic Summer Atmospheric profile has been used which is representative of the spring case [*McClatchey et al.*, 1972]. Total ozone column is set to 365 DU, a typical value between the higher spring values and the lower summer values. The Subarctic summer ozone profile is scaled accordingly. The aerosol is of marine type with a total optical depth of 0.08 at 550 nm [*World Meteorologial Organization*, 1986]. A surface albedo of 0.03 is assumed which is typical for most snow-free surfaces, and topography is not considered. In order to study the pure effects of clouds and their temporal variability, surface albedo, aero-

Table 1. Relation Between Cloud Optical Depths τ and Cloud Geometrical Thicknesses Δz

τ	Δz, m
0–2	40
2–5	90
5–12	220
12–30	540
30–75	1350
75–120	2350

sol, ozone, and profiles of the meteorological parameters are kept constant in all calculations.

[26] Starting with horizontal two dimensional distributions of cloud optical depths taken from NOAA/AVHRR (as explained above in section 2.2) profiles of microphysical cloud properties were constructed. UV radiation is mainly affected by the integrated optical depth while the vertical distribution and droplet size is of minor importance, especially when compared to the larger geometric (3-D) and temporal effects. Here we assumed the stratocumulus size distribution shown by *McCartney* [1976] with a particle concentration $N = 360$ cm^{-3} and an effective radius $r_{\text{eff}} = 7$ μm. The single scattering properties stem from Mie calculations. Assuming constant cloud properties with altitude and fixing the cloud base at 800 m above MSL we obtained cloud top heights which are divided into six classes in order to produce a manageable number of vertical levels (see Table 1).

[27] This approach has already been described and used by *Degünther and Meerkötter* [2000] and *Meerkötter and Degünther* [2001].

3. Diurnal UV Cycles and Time Samplings

[28] This section deals with diurnal UV cycles in relation to time samplings and to radiative transfer aspects.

[29] The repeat cycle of a satellite is a key aspect in accounting for the diurnal variability of clouds for the computation of surface UV daily doses. Geostationary satellites like MSG, Meteosat, or GOES have a time resolution of 15 to 30 min (apart from their rapid scan services), while polar orbiting satellites like NOAA, ENVISAT, or Terra/Aqua have a repeat cycle of ground track typically between 3 and 16 days, although (depending on latitude and swath width) sometimes more than one orbit per day covers the area of interest.

[30] The highest time resolution simulated in this study (see section 3.1) is 15 min according to the cloud input data set illustrated in section 2.2. This time sampling will be called reference time sampling. Different time resolutions can be produced by choosing a subset of the cloud fields according to the two procedures introduced in sections 3.3 and 3.4. The first one describes a time sampling associated to geostationary; the second one describes a time sampling for polar orbiting satellites.

3.1. Reference Daily Doses

[31] UV dose rates computed for every pixel with the highest time resolution of 15 min represent the building blocks for the reference daily doses. They serve as a benchmark for estimating the accuracy of every other calculation. Reference daily doses for each of the 225 pixels are computed from dose rates by integrating this full data set from sunrise to sunset, interpolating linearly between the points. In contrast to this reference time sampling, "partial time sampling" will denote any other time sampling that does not fully exploit the maximum time resolution of 15 min.

3.2. Satellite Algorithms

[32] The characterization of cloud effects on surface UV irradiance and irradiation by means of cloud modification factors (cloud transmissions or cloud correction factors) is widely used [*Lubin and Frederick*, 1991; *Eck et al.*, 1995; *Peeters et al.*, 1998; *Matthijsen et al.*, 2000; *Krotkov et al.*, 2001; *Calbó et al.*, 2005]. These are computed by taking the ratio between the actual and the corresponding clear-sky dose rate, i.e.,

$$\text{CMF}(t) = \frac{\text{cloudy dose rate at time } t}{\text{cloudless dose rate at time } t}.$$

The CMFs, representing cloud transmission at a given time t, are then assumed to be constant during the day or to vary linearly when more than one cloud measurement is present during the course of the day. Multiplication with the appropriate cloud-free dose rates yields the diurnal cycle of UV radiation for the chosen time sampling. Through integration over time, interpolating linearly between the points, the daily dose value is obtained. This procedure, apart from saving computational time, has the advantage of accurately accounting for the clear-sky UV cycle (see for instance Figure 5 for $t \leq 1000$ CET and $t \geq 1800$ CET),

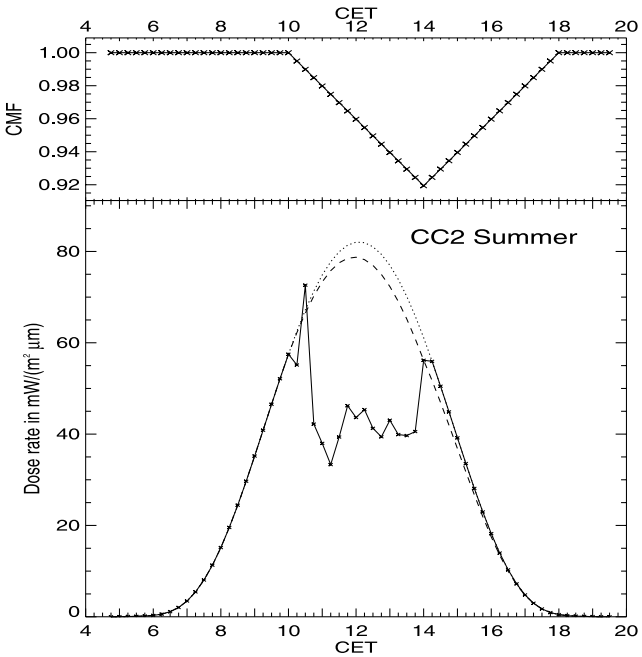

Figure 5. Three-dimensional diurnal UV cycle for the central pixel of cloud cycle CC2 in summer. (top) Cloud modification factors computed from slots at 0600, 1000, 1400, and 1800 CET (4 hour sampling). (bottom) The full line shows piecewise linear interpolation between all dose rates (small "x"-symbols) in the full resolution, the dashed line represents the daily cycle for the four real slots mentioned above. For comparison, the cloudless diurnal cycle is shown as a dotted line.

which at the same time represents the upper bound of every UV dose rate, as expected in a 1-D (IPA) radiative transfer perspective. Thus the influence of clouds on UV radiation is interpolated linearly such that the resulting UV cycles, constrained to a physically meaningful range, vary continuously between successive cloud measurements.

3.3. Time Sampling of Type 1 (Geostationary)

[33] Type 1 time sampling exhausts the possibilities given by a geostationary satellite. Daily doses are constructed by extracting dose rates separated by definite time intervals from the reference UV cycle. In this study, these time intervals range from 30 min to 4 hours increasing in steps of 15 min. This procedure is called, for instance, "30 min time sampling" and altogether there are 15 possible time intervals. For each selected dose rate a CMF is computed like in section 3.2. The CMFs are interpolated linearly in steps of 15 min.

[34] The bottom plot in Figure 5 shows an example of a diurnal cycle of surface UV radiation (3-D) associated with the central pixel in the area for the CC2 cloud cycle in summer. Depicted are dose rates for the full 15 min resolution (section 3.1) as small "x"-symbols connected by solid straight lines. As expected, this line coincides with the dotted one indicating clear-sky UV levels in the morning and in the afternoon (section 2.2). Around noon, clouds are present and a typical 3-D effect can be noticed as the cloudy dose rate exceeds the cloudless one at 1030 CET (section 2.3), represented as a dotted line. The dashed line represents a diurnal cycle of UV radiation determined by four dose rates at 0600, 1000, 1400, and 1800 CET. All dose rates have been calculated by means of the CMFs shown in the top plot of the same Figure. This is an "unfortunate" case where the 4 hour sampling basically misses the whole cloud present around noon.

[35] Finally, for every cloud field and for every pixel, 15 different daily doses are obtained according to the sampling with 15 different time intervals.

[36] Each m min time sampling has in principle $n = m/15$ different realizations. For example, if dose rates are chosen every 60 min, this leads to $4 = 60/15$ different sampling realizations, starting (in spring) with slots at 0600, 0615, 0630, or 0645 CET. Different realizations can yield very different results, depending on which dose rates are used. This is especially true for a "poor" time sampling that extracts dose rates from the reference UV cycles in large time intervals.

[37] In the following sections, results corresponding to a temporal sampling of type 1 will denote results that correspond to the full set of realizations, in the sense of a worst-case analysis. When dealing for instance with maximum deviations between the reference daily doses and the daily doses stemming from the 4 hour time sampling, actually maximum deviations between reference daily doses and the full ensemble of 4 hour time samplings (made up of 16 realizations) are meant.

3.4. Time Sampling of Type 2 (Polar Orbiting)

[38] The probing associated with polar orbiting satellites is called type 2. It is characterized by a restricted availability of cloud probes that are assumed to be sensed around noon. For the corresponding daily doses, henceforth denoted doses of type 2, three overpass times are defined: 1000, 1145, and 1330 CET (typical 105 min orbits). Daily doses from one overpass are based on the assumption that the cloud field sensed at one of these overpass times is present from sunrise to sunset without modifications. Thus with these temporally constant cloud fields three UV daily cycles (corresponding to the three single overpasses) are computed in time steps of 15 min by using the appropriate solar zenith and azimuth angles. Daily doses from two or three overpasses are computed instead by combining two or three of these UV daily cycles with each other, respectively. For instance, when combining the 1000 CET overpass with the 1145 CET overpass, all dose rates that correspond to times up to 1045 CET are extracted from the UV daily cycle of the first overpass. From the UV daily cycle of the second overpass all remaining dose rates are taken to cover the rest of the day (UV dose rates for 1100 CET and later). Piecewise linear interpolation followed by integration over time then provides daily doses for every pixel.

[39] In the following, results related to the time sampling of type 2 will be grouped according to the number of overpasses used in the computation of the daily doses. In the same manner as for type 1 samplings, they will always refer to the worst case that can be constructed using the given number of overpasses, especially when different combinations are possible (e.g., two overpasses correspond to the worst result among those built using the 1000 and the 1145 CET, the 1000 and the 1330 CET, and the 1145 and the 1330 CET overpasses).

3.5. Diurnal UV Cycles in Spring and Summer

[40] The diurnal variations of UV radiation are determined by the course of the solar zenith angle (Figure 1) and the changing physical and optical properties of the cloud structures (Figure 2). Owing to the larger solar zenith angles the photon path is longer in spring than in summer resulting in an increased attenuation. Moreover, the probability that the direct sun reaches the ground through the clouds is smaller in spring. This also reduces the occurrence of situations where multiple scattering enhance UV levels with respect to the clear-sky case (see section 2.3).

[41] The solid line in Figure 6 shows the 3-D (top) and IPA (bottom) diurnal cycles of surface UV dose rates corresponding to the cloud cycle CC1 for the central pixel in spring (left) and summer (right). Apart from the longer illumination time in summer, it is obvious that the spring values are more than one order of magnitude smaller and that the 3-D enhancement of surface UV above the clear-sky curve occurs only in summer. Furthermore, the 3-D summer curve shows a more pronounced variability than the 3-D spring curve that hampers the precise estimation of UV daily doses. The longer illumination time, instead, together with the steeper run of the solar zenith angle shown in Figure 1, can be seen as an advantage as well as a disadvantage. When a part of the diurnal UV cycle is not correctly accounted for, in summer this error can be more easily compensated by an accurate estimation of the rest of the day. On the other side, it is more difficult in summer to derive accurate UV daily doses with a limited number of cloud probes.

[42] In the IPA case (Figure 6, bottom), surface UV radiation for every model pixel at a given time is determined

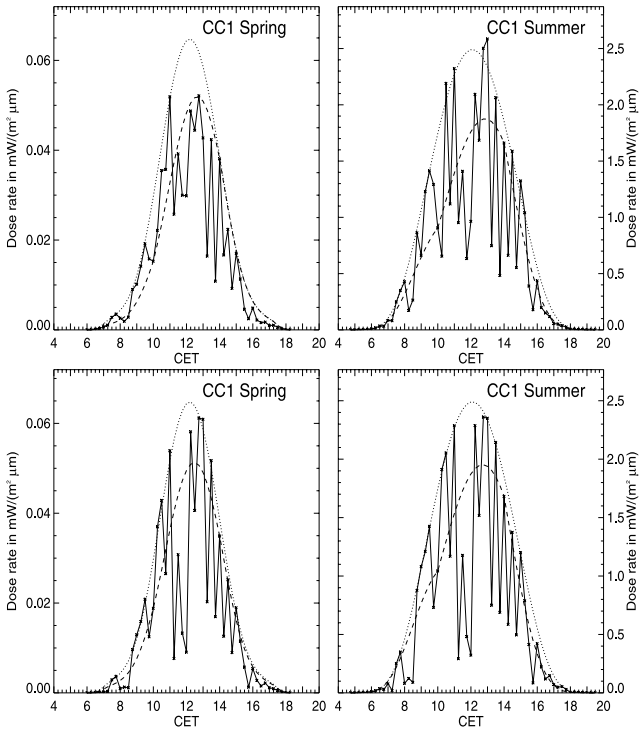

Figure 6. (top) Three-dimensional and (bottom) IPA diurnal UV cycle (solid line) for the central pixel of cloud cycle CC1 for spring (left) and summer (right). For comparison, the clear diurnal cycle is shown as dotted line and a 4 hour time sampling of type 1 as dashed line. Please note the very different ranges of both plots.

by cloud optical and physical properties that are the same for the corresponding spring and summer solar zenith angles since every pixel is considered separately. However, longer photon paths in spring lead again to reduced surface UV dose rates. Therefore the curves are alike in both seasons such that a limited temporal sampling leads to similar type 1 curves (dashed lines in Figure 6).

4. Results: 3-D Versus IPA

[43] Radiative transport is three dimensional in nature and can be rigorously simulated by means of different codes (MYSTIC [*Mayer*, 1999, 2000], SHDOM [*Evans*, 1998], GRIMALDI [*Scheirer and Macke*, 2001; *Macke et al.*, 1997]). However, the operational computation of 3-D daily doses is still not possible due to the high requirements on CPU time. Thus usually approximations are used, like the IPA presented in section 2.3.

[44] In this section, the influence of this approximation on daily doses is investigated when the full time resolution (15 min) of available cloud input data is exploited. IPA reference doses are compared to 3-D reference doses: Section 4.1 is devoted to relative deviations of IPA daily doses with respect to 3-D ones, while section 4.2 shows correlations between them. Section 4.3 is concerned with the effect of spatial averages on the accuracy of IPA daily doses.

4.1. Accuracy Limits

[45] For both spring and summer, relative deviations of IPA daily doses with respect to 3-D daily doses are investigated when the full time sampling of 15 min is used. Figure 7 shows mean (crosses), minimum and maximum (vertical lines) relative differences, as well as standard deviations (polygons). The statistical ensemble is given by the 225 pixels inside the investigated area.

[46] The largest temporal and spatial variability among all cloud cycles characteristic of CC1 is reflected in the largest IPA inaccuracy. Its mean relative difference reaches 9%, its maximum discrepancy is as high as 24% and its root mean square deviation is 5%. All other cycles produce smaller deviations, especially CC6, although it coincides with CC1 for almost all times except noontime, where CC6 is cloud-free and the IPA gives correct results.

[47] The most pronounced spatial homogeneity of daily doses (see minimum, maximum, and rms in spring and summer) is obtained for CC2, where IPA and 3-D radiative transport for clear sky yield equal values (in the range of precision presented in Figure 4) for most times. On the other hand, this should be even more true for CC5, where the number of clear-sky slots is even larger. However, results for CC5 are not particularly good: The spatial and temporal variability during noontime is stronger (broken clouds) than in CC2 (overcast) and produces large errors that cannot be "compensated" by the good accuracy of the cloud-free slots, especially in spring. The longer illumination time in summer mitigates these results.

[48] Unexpected is also at first sight that CC3 yields relatively inaccurate daily doses although this cloud cycle always presents full cloud cover that is constant in time. However, even in this case, photons tend to travel from regions with high to regions with low optical thickness, a

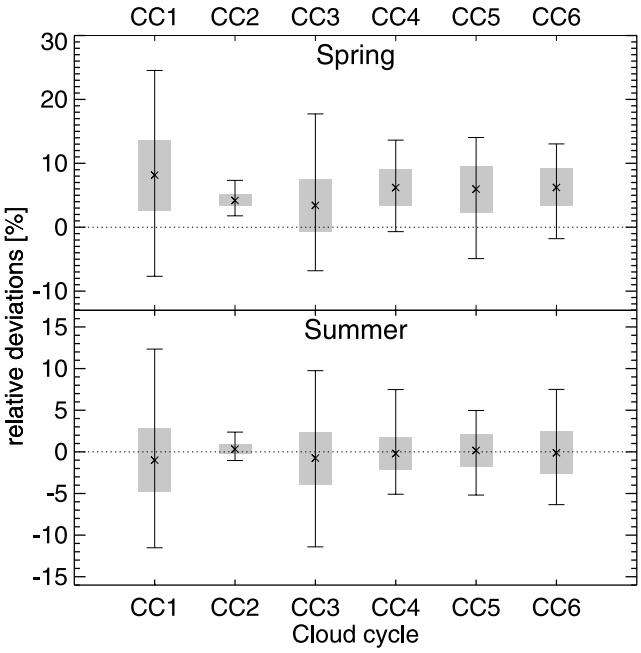

Figure 7. Comparison of IPA daily doses computed with the full 15 min time sampling with respect to 3-D daily doses. Crosses denote mean relative differences; vertical lines denote minimum and maximum relative differences; polygons denote standard deviations. Please note the different scales.

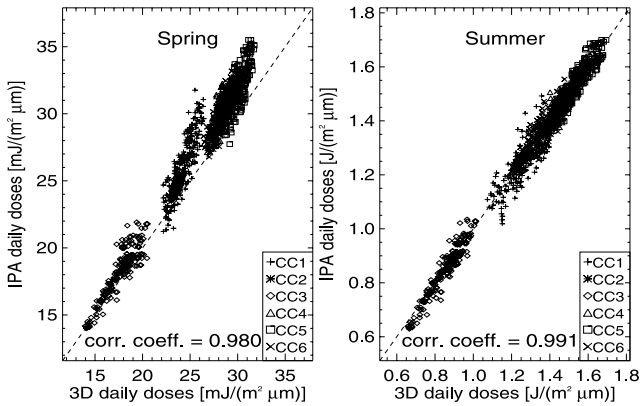

Figure 8. Scatterplot of reference daily doses: IPA versus 3-D for all clouds. The dashed line is the y = x line.

phenomenon that is not considered in the IPA assumption and leads to the observed discrepancies.

[49] An effect common to all cloud cycles is represented by the higher deviations in spring than in summer. Not only extrema are larger, but also mean values. While in summer an average over the whole area yields differences close to zero, in spring mean IPA daily doses always overestimate the reference 3-D value: The bias ranges from 3% to 9%. Two aspects concur to explain this effect: On one side the slight overestimation of the IPA model of 3-D dose rates (Figure 4), on the other, and most important, is the fact that the effective cloud cover seen by photons on slanted paths in spring is higher than in summer for the 3-D model. On the contrary, they do not vary for the IPA model due to its very definition. Thus IPA radiative values are higher than 3-D ones in spring (see also section 3.5).

[50] In summary, with the ideal temporal sampling the IPA assumption leads to discrepancies up to 25% in spring and 13% in summer. Three-dimensional effects cause larger differences in single UV dose rates (exceeding 160% in spring and 210% in summer for the investigated cloud cycles). However, these are significantly reduced when irradiances are integrated over time and do not play an important role for time-integrated doses. Even if a cloud probe every 15 min is used, uncertainties as large as 25% in spring and 13% in summer have to be expected for broken cloud conditions, for daily doses. This is a principle limitation for satellite-based algorithms and must be considered especially when comparing UV doses to ground measurements.

4.2. Correlations

[51] The deviations discussed in section 4.1 suggest that daily doses of each pixel are not very strongly affected by 3-D effects, at least when comparing with the possible discrepancies of IPA and 3-D dose rate values. This is confirmed by Figure 8 showing a scatterplot of IPA and 3-D doses for spring (left) and summer. Cloud cycles are grouped according to the temporal evolution of their cloud cover: Mainly cloud-free cloud cycles like CC5 produce large values; those with higher cloud cover yield smaller daily doses. The observed spring overestimation (Figure 7) is obvious. The correlation coefficient is high (0.980). In summer its value rises to 0.991 and the daily doses lie on the y = x (dashed) line. This means that 3-D radiative effects are averaged out to a certain extent (see also section 4.1) by integration over time.

4.3. Spatial Averages

[52] In the following, the effects of spatial averaging on IPA daily doses are illustrated for the ideal 15 min time sampling. *Meerkötter and Degünther* [2001] and *Scheirer and Macke* [2001] have shown that spatially averaged IPA dose rates, and thus IPA daily doses, approach the mean 3-D dose rate and the mean 3-D daily dose, respectively, over the same area when the averaging domain is large enough. Here we compare spatial averages of IPA daily doses with nonaveraged 3-D values. When averaging over the whole model area, section 4.1 has already shown that 3-D effects are smoothed out such that they turn out to be of less importance on a daily dose level. This part of the study is intended to yield a contribution to the interpretation of comparisons between local, punctual surface UV measurements and corresponding satellite-based values. An aspect worthwhile to be discussed is to which extent the spatial smoothing can account for temporal cloud variations.

[53] Again, IPA daily doses derived from the 15 min input data sets are considered. Spatial averages of them are computed for areas of 1×1, 3×3, 5×5, 7×7, 9×9, 11×11, 13×13, and 15×15 pixels centered around each pixel (moving averages). Then the maximum deviations between these averages and the reference 3-D value of the center pixel in the averaging area are investigated. Note that due to the periodic boundary conditions, the largest averaging area corresponds to averaging over an infinite region. The 1×1 box corresponds instead to no average and renders the maximum values shown in Figure 7.

[54] Averaging length denotes the side length (in pixels or kilometers) of the averaging square.

[55] Spatially averaged daily doses obtained with the full temporal sampling are compared with those obtained for a single pixel (the center pixel of the averaging box) in Figure 9. The maximum relative deviations shown here are very similar in summer and spring, apart from the values corresponding to no averaging (averaging length 1), where the better agreement in summer already exposed in section

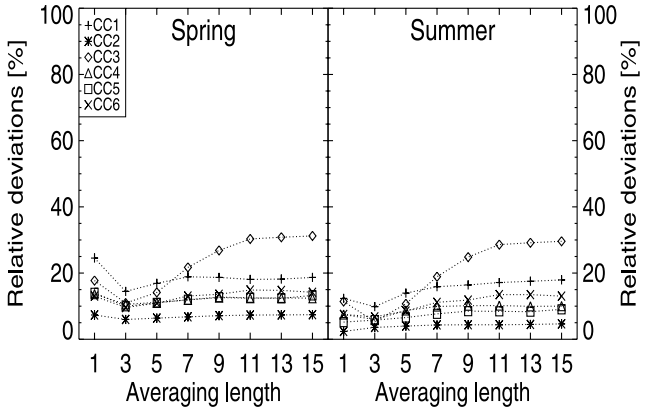

Figure 9. Averaged IPA doses versus reference 3-D value for the center pixel of each averaging area. Maximum relative deviations are shown for all cloud cycles in spring (left) and summer.

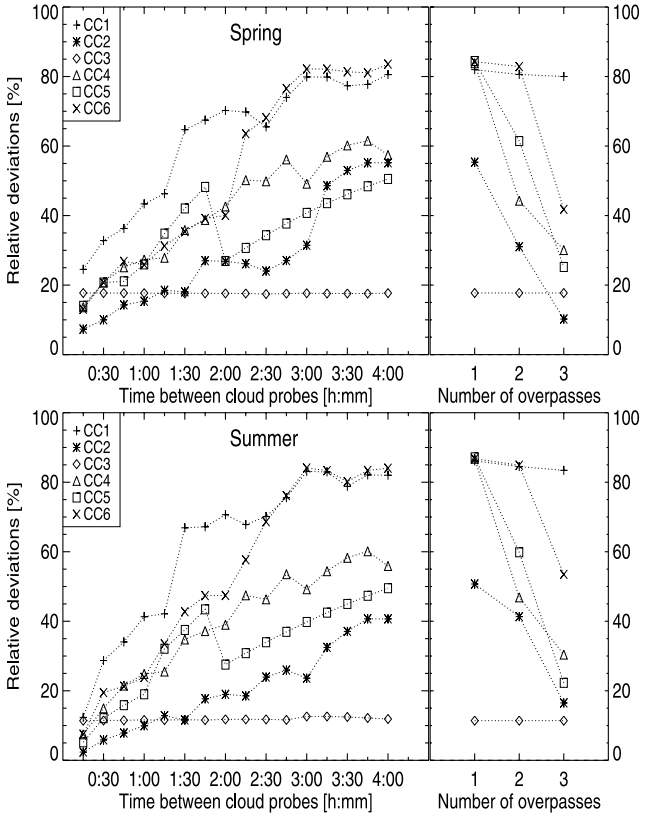

Figure 10. Maximum deviations of IPA doses from the reference 3-D values for every cloud cycle and given time samplings for the (top) spring and the (bottom) summer day. The left panels refer to the temporal sampling of type 1, the right panels to the sampling of type 2.

4.1 emerges again. The curves in Figure 9 initially decrease when a mean over the original (nonaveraged) values is taken (3×3). This is most clear for the spring values. Then, maximum deviations are mostly characterized by an increase with averaging length for all cloud cycles. This means in particular that agreement does not improve when IPA doses are averaged over larger areas. In contrast, it becomes worse even though this increase does not exceed 5% and maximum deviations always stay below 20%. Such low values result from the fact that daily doses are already the product of a time integration smoothing out the spatial variability within the area: An additional average has only little impact. The large increase for CC3 with increasing averaging length is easily explained: Averaging over time does not improve the agreement, as the clouds are constant with time. In contrast, spatial inhomogeneities are persistent (as, e.g., in the case of orographic clouds) and an increase in the averaging area means including more pixels which are systematically different from the center pixel.

[56] In spring, mean relative differences (not shown) range from 3.5% for CC3 and 4.2% for CC2 up to 8.5% for CC1, and about 6% for all other cloud cycles. The dependence on the averaging length is smaller than 1%. In summer, the variability is even smaller and all cloud cycles do not exceed 0.85% mean relative difference. Standard deviations are small in both seasons: Worth mentioning are CC1, whose rms differences vary from 2.4% to 4.9% in spring and from 3.7% to 7.2% in summer but also CC3, with rms values between 2.5% and 9.6% in spring and between 1.6% and 10.5% in summer. The remaining cloud cycles present smaller variability of their rms between 1% and 3.5% in spring and 0.7% and 5.3% in summer (maximum 2% in spring and 2.8% in summer).

[57] In summary, spatial averaging of satellite-derived daily doses improves the agreement with ground-based observations only if the averaging length is not too large. Systematic differences in cloud properties over the averaging area can easily cause larger differences if the averaging area is chosen too large.

5. Results: Time Sampling Effects

[58] The lack of observations of cloud properties with high time resolution requires further assumptions to compute daily doses of (UV) radiation. In this section we investigate the uncertainty of estimated UV daily doses when the full time resolution (15 min) is not available or cannot be exploited.

[59] Section 5.1 focuses on relative deviations from the reference daily doses for both type 1 and type 2 daily doses. Particular attention is paid to maximum deviations that are obtained from the ensemble of all model pixels and for a specific time sampling. Thus these results highlight one pixel in the entire model area. The statistical distribution of daily doses over the model area is addressed by investigating the fraction of pixels deviating by less than ±20% from the reference daily dose (section 5.2). Finally (section 5.3), the effect of spatial averages of IPA doses on the accuracy is investigated like in section 4.3.

5.1. Maximum Uncertainties

[60] Here, maximum deviations of the IPA daily doses based on limited temporal cloud samplings from the corresponding 3-D reference doses with full time resolution are discussed with the aim to determine the maximum error.

[61] In Figure 10 the modulus of maximum relative deviations from the reference case is shown for the geostationary and the polar sampling. Selected are the maxima over all pixels and over the whole set of possible realizations for a given sampling.

[62] Starting with type 1 doses, the left panels of Figure 10 show, in general, maximum relative deviations that increase with decreasing temporal resolution. In more detail, however, the curves are not characterized by neither a monotonic nor a linear increase. This means that time samplings of type 1 with larger probing time intervals are not necessarily worse than others with smaller sampling times. However, it suggests that a 15 min sampling difference plays a major role for shorter samplings ($\leq$1 hour 15 min), while poor scannings ($\geq$3 hours) are approximately equivalent. Furthermore, curves of individual cloud cycles have very different shapes while differences between spring and summer are small. This indicates that the relative deviations of type 1 doses from the reference case are mainly dictated by the cloud cycles themselves, while differences related to sun illumination geometry (including the 3-D effects discussed in section 4.1) play a minor role. Particularly

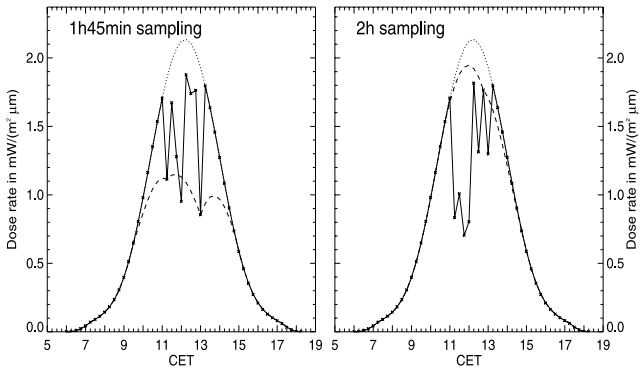

Figure 11. Diurnal UV cycle (IPA) for CC5 in spring. (left) Pixel (8,9) with 1 hour 45 min type 1 sampling (dashed line). (right) Pixel (10,8) with 2 hour type 1 sampling (dashed line). These samplings yield the largest uncertainty plotted in Figure 10 for the CC5 scenario. In both panels, the solid line denotes the UV cycle at the highest temporal resolution of 15 min while the clear diurnal cycle is shown as dotted line.

difficult is the approximation of spatially and temporally highly inhomogeneous cloud cycles (CC1, CC6).

[63] In general, short temporal samplings extract UV dose rates more or less in a random way from the diurnal cycles of radiation such that all features of the given cloud cycles are mirrored. This way, daily doses are produced that overestimate or underestimate the reference 3-D values in a comparable manner. When the time step between successive cloud probes becomes larger the temporal and spatial characteristics of the single cloud cycles are crucial. In particular, it is possible that only special features of the clouds are sensed thus leading to larger discrepancies or to rapidly changing uncertainties. Figure 11 illustrates such an effect considering two successive time samplings that lead to a large accuracy increase for CC5 in spring. Here, peaks of the mean optical thickness around 1115 CET and 1245 CET are selected by the 1 hour 45 min temporal scanning, while this is no longer the case for coarser samplings because then the two probing times lie too far away from each other. The large uncertainty increase in CC2 or CC5 in spring between 3 hours and 3 hours 15 min or 2 hours and 2 hours 15 min, respectively, takes place because noontime clouds are no longer sensed when the cloud probe separation is too large. For CC1, the abrupt maximum deviation increase by about 20% from the 1 hour 15 min to the 1 hour 30 min temporal scanning interval in spring occurs when type 1 samplings select exclusively small dose rates, i.e., clouds with large optical thickness. In contrast, the CC3 spring accuracy is almost independent of the temporal sampling: It amounts to 18% in spring and 12% in summer. This cloud cycle consists of a stratus with a spatially inhomogeneous optical depth that does not vary in the course of the day. All pixels show smooth diurnal UV cycles and the sampling times are of little importance. For CC2, samplings between 1 hour 45 min and 2 hours 45 min (or even 3 hours) all lead to similar accuracies: Here morning and afternoon are well estimated (each with one probe), while noontime is overestimated (also with one probe), each time in a similar manner. The most striking property of CC4 is its relatively steady uncertainty increase as a function of sampling interval with maximum deviations that exceed 60% for poor time samplings. In this case, morning and afternoon are long enough to be considered at least partially and are always sampled. Furthermore, there is always a clear slot before noon that enables to approximate the noon dose rates relatively well. Largest deviations appear when a slot with thick clouds just after 1200 CET reduces the contribution of noontime to the daily dose.

[64] The corresponding results for summer (Figure 10, bottom) are comparable to or smaller than those for spring (top), especially for the poorest samplings. Prime examples for lower deviations during summer are CC3 and CC2. Reason for the former cloud cycle are reduced shadow displacement effects (−7%) in summer, while for the latter (maximum deviation for the 4 hour sampling of 40% in summer against 55% in spring) is the increased daylight duration. In fact, in both cases noontime (1045–1200 CET) is completely cloud-free for the worst sampling. Owing to the lower weight of the noon dose in summer this error plays a larger role in spring. In fact, in spring (summer) the time between 1000 and 1400 CET contains 74% (63%) of the entire cloud-free daily dose. Considering clouds as well, the noon doses of CC1-CC6 represent 64–80% of the full daily doses in spring and 53–71% in summer (see Table 2). The lower values in summer are controlled by the longer illumination time on one side and the steeper daily cycle of radiation on the other side (see section 3.5). This fact can sometimes explain larger differences in summer with respect to spring. This is observed, e.g., for the 1 hour 30 min sampling for CC6 (uncertainty of 35% in spring and 43% in summer) where the morning and afternoon doses can be better approximated in spring.

[65] Type 2 daily doses (right panels of Figure 10) generally show a steep decrease with increasing number of overpasses such that accurate results can be achieved with only three cloud probes. This is not true, however, when high spatial variability is coupled with high temporal variability as in CC1. Here, there is always at least one sampling corresponding to thick clouds such that the resulting sampling cannot account for the unhindered sun incidence every now and then and heavily underestimates the real daily dose.

[66] Furthermore, the spring values corresponding to one overpass are very similar to those of type 1 obtained with a cloud probing in 4 hour intervals for CC1, CC2, and CC6, or worse for CC4 and CC5 (by almost 30–35%). This indicates that only one single overpass, even during noontime, is unlikely to be representative of the daily cloud cycle. Only when the number of overpasses increases, these snapshots become characteristic of the cloud cycle during noontime. For this reason, the bad accuracy of CC6 type 2 doses for one and two overpasses significantly improves when also a cloud-free probe (1145 CET) is selected. With

Table 2. Noon Dose (1000–1400 CET) in Percent of the Corresponding Three-Dimensional Daily Dose

	Clear-Sky	CC1	CC2	CC3	CC4	CC5	CC6
Spring (mean)	74	77	64	75	77	72	80
Summer (mean)	63	70	53	65	69	63	71

three overpasses the type 2 spring doses deviate from the reference doses by 45% (CC6), 30% (CC4), 25% (CC5), and 10% (CC2) at the most. To obtain type 1 daily doses that do not exceed these values, a time interval between cloud probes shorter than 30 min for CC2, 1 hour 15 min for CC4, 45 min for CC5, and 2 hours for CC6 has to be chosen in spring. However, these type 1 samplings are based on a number of cloud probes between 6 (2 hours) and 24 (30 min). Better results would be achieved by spreading these cloud probes over noontime. The reason why noon cloud probes contain more valuable information is illustrated again by Table 2 and the explanation above.

[67] Like for type 1 samplings, the shape of the curves is similar in both seasons, thus pointing at corresponding effects related to the cloud cycle characteristics. As far as absolute values are concerned, notice that maximum deviations in summer for three overpasses are similar to those in spring except for two cloud cycles (excluding CC3 whose behavior can be explained as for type 1 samplings). For CC2 (17%), this is caused by a slightly worse approximation of the afternoon dose by means of the cloudy 1330 CET overpass; for CC6 (55%), the reason is similar and refers to a worse summer approximation of both morning and afternoon doses through one overpass each and to the increasing relative weight of these partial doses.

[68] The type 1 samplings that yield the same accuracy as the best type 2 sampling in summer are very similar to those in spring, although the number of cloud probes needed is larger in summer due to the longer daylight duration.

5.2. Typical Uncertainties

[69] In the previous section, the pixel with the highest inaccuracy for a given sampling has been identified. In order to gain an overview about the behavior of all pixels in the area under study practical statistical considerations are addressed in the following.

[70] Figure 12 shows the fraction of pixels in the entire area whose IPA results deviate from the 3-D reference daily doses by less than 20% as a function of temporal resolution. This value represents the typical difference between the model results based on one cloud probe and ground-based measurements according to *Martin et al.* [2000]. These plots show the minimum of all possible realizations (see again sections 3.3 and 3.4). In the following a ±20% relative difference from the reference daily dose is called a "good accuracy."

[71] We start with CC3: Since maximum deviations are always smaller than 20% (Figure 10), it is obvious that all pixels inside the area under study have good accuracy, independently of time sampling and season.

[72] The other cloud cycles have different and more complex behaviors. Looking at type 1 samplings first, it can be seen that in general an increase of the time step between successive probes results in a reduction of the number of pixels with good accuracy, as expected. There are cloud cycles for which even with the 1 hour sampling approximately 95% of the pixels have good accuracy in spring (CC2, CC3, CC5, CC6). However, with this probing interval, no more than 70% of CC1 pixels have this quality, and for CC4 this percentage is around 85%. In order to achieve a good accuracy for at least half of the pixels in spring one has to consider a type 1 sampling of 1 hour for

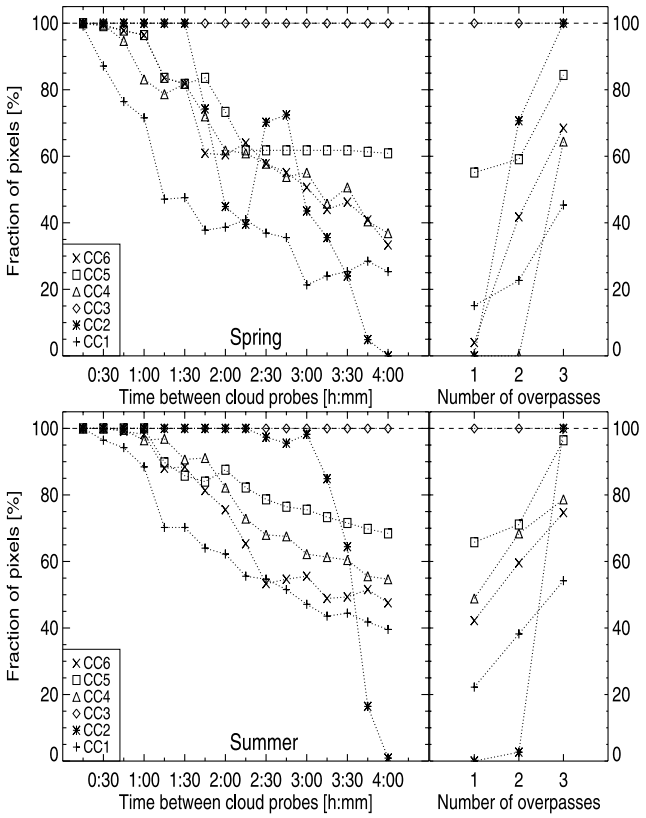

Figure 12. Fraction of IPA doses with an uncertainty (w.r.t. 3-D daily doses) less than 20% for every cloud cycle for the spring (top) and the summer (bottom) day. The left panels refer to the temporal sampling of type 1, the right panels to the sampling of type 2.

CC1, 1 hour 45 min for CC2, 3 hours for CC4, and 2 hours 45 min for CC6. The remaining two cloud cycles (CC3 and CC5) always fulfill this property (i.e., the 4 hour sampling is sufficient).

[73] Comparing Figure 12 and Figure 10, striking features of the curves in the left panel of one figure are not encountered in the other one, and vice versa. This indicates that no direct correlation is possible and that the worst realization under one aspect is not necessarily the worst under the other. Consider for example the irregular run of the CC2 curve in Figure 12 that is not mirrored in Figure 10. Similarly, CC1 is not always the most difficult case in Figure 12, and CC6 is closer to CC4 or CC5, in particular for poor time samplings.

[74] Again of course the curves in Figure 12 are affected by the characteristics of each cloud cycle. A given type 1 sampling is able to estimate the UV daily dose with a better or worse accuracy than its predecessor depending on whether certain cloud features can be correctly accounted for or not. This is particularly apparent for CC2 in spring: successive temporal samplings yield very different results depending on how the cloudy noontime is represented. In summer, only the last type 1 samplings produce very few good quality pixels for CC2 as a proof of the different weight of the noon dose with respect to the rest of the day. Even when cloud cycles are similar, like CC2 and CC5, they can show different behaviors: Type 1 samplings poorer

than 2 hours 15 min lead to almost constant fractions of good quality pixels for CC5, while CC2 is characterized by large variations. This is mainly caused by the shorter period of cloud appearance in CC5 (1115–1300 CET), by the smaller cloud cover, and by the lower cloud optical thicknesses. From the 2 hours 15 min to the 3 hours 30 min sampling the constant CC5 curve in Figure 12 (spring) is caused by the reproduction of cloud-free or almost cloud-free doses for every pixel (i.e., the cloudy slots are not sensed due to the position of the probing times). In summer this almost absolute constancy translates into a small decrease from about 80% down to about 68%. These larger values compared to spring again indicate the reduced relative weight of the noon dose.

[75] In general, summer is characterized by slower decreases than spring, more homogeneity (i.e., smaller differences between the single cloud cycles) and larger fractions of good accuracy pixels. Three cloud cycles (CC3, CC4, CC5) actually never fall below 50%; to obtain good accuracy for at least half of the pixels in the remaining cases the cloud fields have to be scanned every 2 hours 45 min (CC1), 3 hours 30 min (CC2), and 3 hours (CC6). This improved overall pixel accuracy which can be reached in summer compared to spring is not mirrored in Figure 10, i.e., although the maximum relative errors in summer are more or less as high as in spring, the fraction of pixels with an accuracy within ±20% with respect to the reference 3-D daily doses is significantly bigger in summer.

[76] The percentage of type 2 daily doses with good accuracy (right panels of Figure 12) shows a steep increase with the number of overpasses. This is particularly striking for CC1, since it strongly contrasts with Figure 10. This indicates that in case of high spatial and temporal variability, as in CC1, three overpasses are not able to noticeably reduce the maximum uncertainties but can improve the overall agreement with the reference doses. Again, in general one or two overpasses are not always sufficient to produce good results for a considerable fraction of pixels. With three overpasses, however, results are always larger than 60% (CC4: 65%, CC6: 68%, CC5: 85%, CC2 and CC3: 100%) in spring, with the exception of CC1 (45%). To reach the same amount of ''good'' pixels as with the three overpass type 2 sampling a 1 hour 30 min type 1 sampling has to be used for CC1, 1 hour 30 min for CC2, 1 hour 45 min for CC4, 1 hour for CC5, and 1 hour 30 min for CC6. The use of one overpass usually yields worse results than the 4 hour type 1 sampling, in contrast to Figure 10.

[77] Similarly as for the type 1 samplings, type 2 samplings yield better results in summer. Good accuracy for at least 50% of the pixels can be obtained for all cloud cycles: For CC4 and CC6 two overpasses are required, three for CC1 and CC2, and one for CC3 and CC5. Except for CC1 (55%), the smallest fraction amounts to 75% when three overpasses are used. The slight increase of CC5 from one to two overpasses already noticed in spring remains, the one showed by CC2 (only in summer) is instead produced by the 1145 and 1330 CET overpasses where the presence of thick clouds leads to strong underestimations, in particular of the morning and afternoon doses that play a more important role in summer. Interesting is also CC4 whose UV doses can be well approximated in summer for almost 50% of all pixels even with one overpass only (1330 CET), while the two cloud-free overpasses yield good results for almost 70% of the pixels. The probing interval required by type 1 scannings to yield better results than three type 2 overpasses are 2 hours 15 min for CC1, 2 hours 15 min for CC2, 2 hours for CC4, 1 hour for CC5, and 2 hours for CC6 in summer. Thus although both sampling types yield better results in summer than in spring, type 2 samplings are not as effective in summer as in spring when compared with type 1 samplings. This is due to the fact that the latter yield a better coverage of the time outside noon that plays a more important role in summer. In any case, it must be noted that all type 1 samplings comparable to the best type 2 results with three overpasses employ more than three slots. Thus under this point of view, using only three cloud probes in the time interval around noon is already very effective in deriving daily doses.

5.3. Uncertainties of Spatial Averages

[78] In this section we investigate how the IPA averages deviate from the reference 3-D value of the center pixel in the averaging area. As usual, the 3-D daily doses derived from the 15 min input data sets build the reference. In the following we consider exemplarily two time samplings of type 1 (1 hour and 3 hours) and all type 2 samplings. The 1 hour type 1 sampling is selected because it already produces large maximum deviations from the 3-D reference doses (Figure 10), although many pixels still have good accuracy (Figure 12). The 3 hour sampling is instead representative of the worst type 1 samplings. The reference sampling has already been discussed in section 4.3 where the averaging procedure has been introduced.

[79] Maximum deviations of averaged IPA daily doses from 3-D reference values are displayed in Figure 13 for spring and summer.

[80] At first, all cloud cycles are discussed for the spring day and for the sampling of type 1 (upper part of Figure 13). For CC3, maximum deviations increase as a function of the averaging length, reproducing the pattern seen in Figure 9. The mechanism is the same as in section 4.3.

[81] The deviations for the 1 hour sampling of all other cloud cycles are almost independent of averaging length. Averaging over 3×3 pixels reduces maximum relative differences from 43% to 22% for CC1, while results for the other cloud cycles are almost unchanged (decreases smaller than 5%). Thus a relevant improvement can only be seen for the most inhomogeneous (spatially and temporally) cloud cycle.

[82] Maximum deviations for small averaging boxes are much larger in the 3 hour time sampling of type 1 (right panel of Figure 13) than in the 1 hour time sampling excluding CC3 (see above). This is caused by the larger uncertainty of this time sampling (see Figure 10). In this case a strong reduction of the deviations is observed when spatial averages are computed over larger areas. This is particularly evident for CC1 and CC6 that show an extremely strong decrease as a function of the averaging length. Noteworthy is also that for the largest averaging area maximum deviations are between 20% and 27% for all cloud cycles (except CC3), thus showing that spatial and temporal characteristics of the input cloud cycles are washed out by the averaging procedure. In fact, inaccuracies

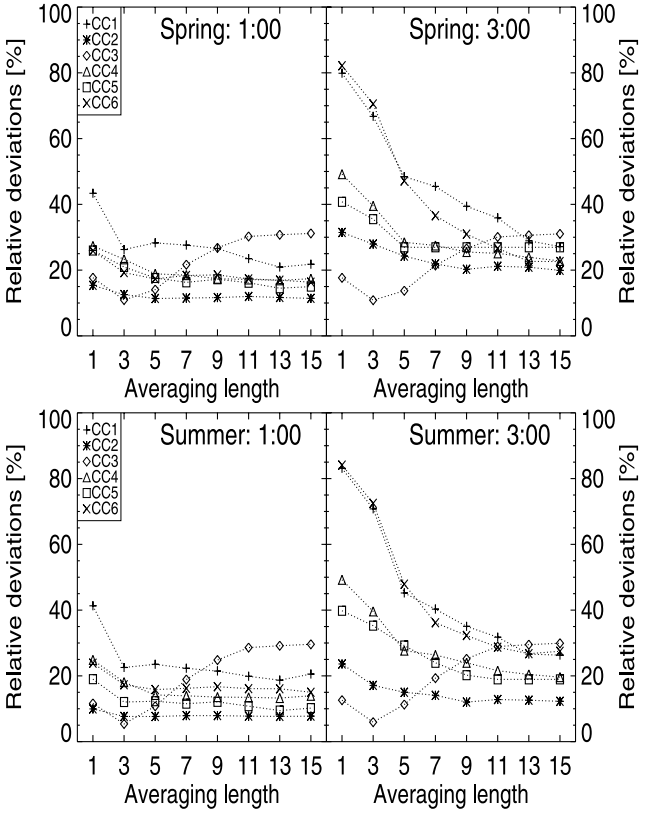

Figure 13. Maximum deviations between averaged IPA and 3-D reference (nonaveraged) daily doses for every cloud cycle for the (top) spring day and the (bottom) summer day (bottom). Both panels refer to the temporal sampling of type 1: The left one uses a time interval of 1 hour and the right one of 3 hours.

of the two type 1 samplings investigated become comparable after averaging over 15×15 pixels.

[83] Time samplings of type 2 are shown in Figure 14. Owing to the reduced number of cloud probes used, type 2 curves are similar to the 3 hour type 1 sampling in Figure 13 and a spatial averaging clearly produces a better agreement to the reference values. The different behavior of CC3 has the same explanation as given above, while for CC2 the choice of the cloud-free overpass at 1000 CET in the leftmost panel in Figure 14 (spring) yields a maximum deviation of 55% from the reference which is valid for all averaging lengths. Similarly, the constancy of CC4 for averaging lengths larger than 5 in the middle panel in Figure 14 is attributed to the choice of two cloud-free overpasses (1000 and 1145 CET).

[84] In all panels of Figure 14 the smallest deviations are obtained for the averaging length of 15: They lie below 55% for one overpass (below 45% in summer), for two and three overpasses they do not exceed 35% in spring and 30% in summer. Except for the one overpass results, where the decrease of maximum relative deviations is almost linear up to the averaging length of 9, the other two panels show that the largest improvement is produced by the 5 × 5 averaging area. This becomes most evident when very inhomogeneous cloud cycles like CC1 and CC6 are observed. For these cases, the most relevant improvement is obtained with three overpasses. Eventually, the combinations of three overpasses with the largest averaging box yields maximum relative deviations that do not exceed 20% except for CC3. These results are even better than the nonaveraged 15 min IPA daily doses plotted in Figure 10.

[85] Summer curves (Figure 14, bottom) are similar to the corresponding spring curves. Hence they are not further discussed here.

[86] It has to be noted that all the cloud field constituents that build a diurnal cloud cycle stem from a single NOAA/AVHRR scene. The cycles are generated in a synthetic way and therefore do not represent a real temporal cloud variation. In this sense, it is only conditionally possible to assert that averaging over a certain area accounts for temporal variation of clouds. The effects that emerge from our model studies are mainly due to statistical features. In case of a real application of deriving daily doses, i.e., when spatial averaging may account for a temporal cloud evolution, at least to a certain degree, better dose estimations may be obtained.

[87] The preceding results show that even methods based on few cloud probes have the potential of accurately estimating UV daily doses. In fact, in our examples three slots seem to be able to satisfactorily account for the temporal cloud variability during the day. An additional smoothing procedure could then always reduce maximum

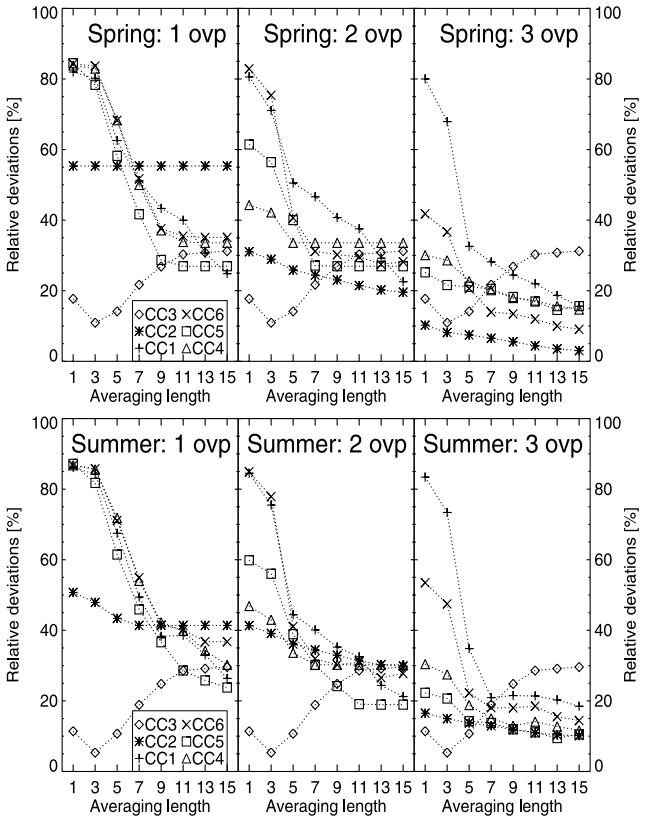

Figure 14. Maximum deviations between averaged IPA and 3-D reference (nonaveraged) daily doses for every cloud cycle and for the (top) spring and the (bottom) summer day. The three panels refer (from left to right) to a type 2 sampling based on one, two, or three overpasses.

deviations to below 30%, in many cases to below 20%, and in some even to below 10%.

6. Summary and Conclusions

[88] Aim of this study is to evaluate the performance of algorithms that compute surface UV radiation from satellite-derived cloud information. In particular, the implications related to limited temporal samplings of cloud fields and the neglect of 3-D radiative effects are addressed, while all other sources of error are excluded. The main results can be summarized as follows:

[89] 1. At the highest time resolution of 15 min the uncertainties of daily doses due to the disregard of 3-D effects are smaller than 25% in spring and 13% in summer. The integration over time strongly reduces the deviations between IPA and 3-D dose rates that can exceed 150% in spring and 200% in summer. IPA and 3-D daily doses are highly correlated, especially in summer. On the other hand, however, the presence of this residual inaccuracy means that even if a cloud probe every 15 min is used, uncertainties as large as 25% in spring and 13% in summer may occur in case of broken cloud conditions. This is a principle limitation for satellite-based algorithms and must be considered especially when comparing UV doses to ground measurements. Furthermore, for low sun conditions (spring), a bias ranging from 3% to 9% remains, even in a temporally homogeneous case like that of a stratus cloud.

[90] 2. A reduced temporal sampling causes larger uncertainties. Maximum relative deviations of geostationary IPA doses from 3-D reference values over the entire area grow in general with the time interval between successive cloud probes but large drops or increments may occur, depending on the cloud cycles. Thus it is hard to find a compromise between computational effort and accuracy. In general, the study shows that the accuracy decrease is rapid for short temporal scanning intervals of type 1 ($\leq$1 hour) and slow for poor time samplings ($\geq$3 hours). Maximum relative differences rise up to 85% for geostationary samplings. Considering polar orbiting doses, the use of one overpass only leads to results that are not better than the poorest (4 hours) geostationary sampling. In most cases, accuracy increases rapidly with the number of overpasses. However, in case of high temporal and spatial cloud variability throughout the day three cloud probes can still be too few to prevent the occurrence of large (>80%) deviations.

[91] 3. The detailed analysis in section 5 stresses the importance of acquiring cloud optical properties during noontime. Concerning computational effort, increasing the number of cloud probes is most efficient during this time. Already a small number of slots during this part of the day yields a much better accuracy than using the same number of slots homogeneously spread during the whole day. This is particularly true for spring. However, in summer the longer daylight duration together with the steeper slope of the solar zenith angle curve imply that an extended time interval around noon should be scanned in order to obtain accurate results. In general, better results are obtained in summer for both sampling types.

[92] 4. Even for the poorest geostationary samplings up to 60% of the pixels in spring and 70% in summer have an accuracy within −20% and +20% from the 3-D reference values. As far as polar orbiting samplings are concerned, only with three overpasses uncertainties smaller than 20% can be always achieved for more than 45% of the pixels in spring and 55% in summer, even in the presence of high spatial and high temporal cloud variability. It is noteworthy that maximum deviations as high as 85% are observed simultaneously with such large fractions of pixels within ±20% accuracy: After all, one can be sure that about half of the pixels in the area under study always have good accuracy.

[93] 5. The estimation of a daily dose can be improved by taking spatial averages. For the reference sampling optimum results are obtained when averaging over a 3 × 3 pixel box while for larger averaging areas accuracy decreases again. In most cases, however, the averaged uncertainties remain smaller than the original (nonaveraged) ones. For poorer samplings larger averaging areas lead to a better agreement to the 3-D reference values. Maximum deviations of IPA daily doses from 3-D reference values decrease for example from 85% to 30% when averaging over the entire model area and using a geostationary sampling of 3 hours. When, however, UV doses are biased due, e.g., to 3-D radiative effects, averaging must not necessarily lead to an improvement. Concerning polar orbiting results, it is interesting that already one noon overpass and an averaging over 15 × 15 km^2 is sufficient (except in one case) to derive daily doses with maximum uncertainties of about 25–35%. This order of magnitude has also been found by *Martin et al.* [2000], *Arola et al.* [2002], and *Meerkötter et al.* [2003] who derived daily doses from one cloud probe only and compared them with surface measurements. Two overpasses and the same averaging box always reduce uncertainties down to 20–35%, while three overpasses together with the smoothing procedure can reduce maximum deviations to below 30%, in many cases to below 20%, and in some even to below 10%. In fact, the question arises whether averaging over a representative cloud field that does not have any direct link neither to the real instantaneous local cloud field properties nor to its temporal variation could be used to obtain an adequate estimation of daily doses. The results about spatial means for instance explain the good results obtained in the work of *Meerkötter et al.* [2003] and give at the same time a recipe for the comparison of satellite-derived UV daily doses and surface measurements.

[94] In summary, very important aspects concerning satellite-based algorithms have been outlined that should be taken into account when computing surface UV daily doses. These aspects include limitations but also possibilities to improve the efficiency of these algorithms such that their performance becomes of even greater interest for many applications.

[95] **Acknowledgments.** This study was partially supported by the EC in the framework of the UVAC project (contract number EVK3-CT-1999-00012). AVHRR data were received and stored at the German Remote Sensing Data Centre (DFD) of DLR.

References

Arola, A., et al. (2002), Assessment of four methods to estimate surface UV radiation using satellite data, by comparison with ground measurements from four stations in Europe, *J. Geophys. Res.*, *107*(D16), 4310, doi:10.1029/2001JD000462.

Bodeker, G. E., and R. L. McKenzie (1996), An algorithm for inferring surface UV irradiance including cloud effects, *J. Appl. Meteorol.*, *35*, 1860–1877.

Cahalan, R. F., W. Ridgway, W. J. Wiscombe, T. L. Bell, and J. B. Snider (1994), The albedo of fractal stratocumulus clouds, *J. Atmos. Sci.*, *51*, 2434–2455.

Cahalan, R. F., et al. (2005), The International Intercomparison of 3D Radiation Codes (I3RC): Bringing together the most advanced radiative transfer tools for cloudy atmospheres, *Bull. Am. Meteor. Soc.*, *86*, 1275–1293.

Calbó, J., D. Pagès, and J. González (2005), Empirical studies of cloud effects on UV radiation: A review, *Rev. Geophys.*, *43*, RG2002, doi:10.1029/2004RG000155.

Degünther, M., and R. Meerkötter (2000), Effects of remote clouds on surface UV irradiance, *Ann. Geophys.*, *18*, 679–686.

Degünther, M., R. Meerkötter, A. Albold, and G. Seckmeyer (1998), Case study on the influence of inhomogeneous surface albedo on UV irradiance, *Geophys. Res. Lett.*, *25*, 3587–3590.

Eck, T., P. Barthia, and J. Kerr (1995), Satellite estimation of spectral UVB irradiance using TOMS derived total ozone and UV reflectivity, *Geophys. Res. Lett.*, *22*, 611–614.

Evans, K. F. (1998), The spherical harmonics discrete ordinate method for three-dimensional atmospheric radiative transfer, *J. Atmos. Sci.*, *55*, 429–446.

Herman, J. R., N. Krotkov, E. Celarier, D. Larko, and G. Labow (1999), The distribution of UV radiation at the Earth's surface from TOMS measured UV-backscattered radiances, *J. Geophys. Res.*, *104*, 12,059–12,076.

Kalliskota, S., J. Kaurola, P. Taalas, J. R. Herman, E. Celarier, and N. Krotkov (2000), Comparison of daily UV doses estimated from Nimbus-7/TOMS measurements and ground-based spectroradiometric data, *J. Geophys. Res.*, *105*, 5059–5067.

Kaye, J. A., and T. L. Miller (1996), The ATLAS series of shuttle missions, *Geophys. Res. Lett.*, *23*, 2285–2288.

Kriebel, K. T., R. W. Saunders, and G. Gesell (1989), Optical properties of clouds derived from fully cloudy AVHRR pixels, *Beitr. Phys. Atmos.*, *62*, 165–171.

Kriebel, K. T., G. Gesell, M. Kästner, and H. Mannstein (2003), The cloud analysis tool APOLLO: Improvements and validations, *Int. J. Remote Sens.*, *24*, 2389–2408.

Krotkov, N. A., R. K. Barthia, J. R. Herman, V. Fioletov, and J. Kerr (1998), Satellite estimation of spectral surface UV irradiance in the presence of tropospheric aerosols: 1. Cloud-free case, *J. Geophys. Res.*, *103*, 8779–8793.

Krotkov, N. A., J. R. Herman, R. K. Barthia, V. Fioletov, and Z. Ahmad (2001), Satellite estimation of spectral surface UV irradiance: 2. Effects of homogeneous clouds and snow, *J. Geophys. Res.*, *106*, 11,743–11,759.

Lubin, D., and J. E. Frederick (1991), The ultraviolet radiation environment of the Antartic Peninsula: The roles of ozone and cloud cover, *J. Appl. Meteorol.*, *30*, 478–493.

Lubin, D., and H. Jensen (1995), Effects of clouds and stratospheric ozone depletion on ultraviolet radiation trends, *Nature*, *377*, 710–713.

Lubin, D., E. H. Jensen, and H. P. Gies (1998), Global surface ultraviolet radiation climatology from TOMS and ERBE data, *J. Geophys. Res.*, *103*, 26,061–26,091.

Macke, A., J. Mueller, K. Nagel, and R. Stuhlmann (1997), A cellular automaton model for cloud formation, in *IRS96: Current Problems in Atmospheric Radiation*, edited by W. L. Smith and K. Stamnes, pp. 234–237, A. Deepak, Hampton, Va.

Martin, T. J., B. G. Gardiner, and G. Seckmeyer (2000), Uncertainties in satellite-derived estimates of surface UV doses, *J. Geophys. Res.*, *105*, 27,005–27,011.

Matthijsen, J., H. Slaper, H. A. G. M. Reinen, and G. J. M. Velders (2000), Reduction of solar UV by clouds: A remote sensing approach compared with ground-based measurements, *J. Geophys. Res.*, *105*, 5069–5080.

Mayer, B. (1999), I3RC phase 1 results from the MYSTIC Monte Carlo model, in *Intercomparison of Three-Dimensional Radiation Codes: Abstracts of the First and Second International Workshops*, pp. 49–54, Univ. of Ariz. Press, Tucson, Ariz.

Mayer, B. (2000), I3RC phase 2 results from the MYSTIC Monte Carlo model, in *Intercomparison of Three-Dimensional Radiation Codes: Abstracts of the First and Second International Workshops*, pp. 107–108, Univ. of Ariz. Press, Tucson, Ariz.

McCartney, E. J. (1976), *Optics of the Atmosphere*, John Wiley, Hoboken, N. J.

McClatchey, R. A., R. W. Fenn, J. E. A. Selby, F. E. Volz, and J. S. Garing (1972), *Optical Properties of the Atmosphere*, 3rd ed., *AFCRL-72-0497*, Air Force Cambridge Res. Lab., Bedford, Mass.

McKenzie, R., G. Seckmeyer, A. F. Bais, J. B. Kerr, and S. Madronich (2001), Satellite retrievals of erythemal UV dose compared with ground-based measurements at northern and southern mid-latitudes, *J. Geophys. Res.*, *106*, 24,051–24,062.

Meerkötter, R., and M. Degünther (2001), A radiative transfer case study for 3-D cloud effects in the UV, *Geophys. Res. Lett.*, *28*, 1683–1686.

Meerkötter, R., B. Wissinger, and G. Seckmeyer (1997), Surface UV from ERS-2/GOME and NOAA/AVHRR data: A case study, *Geophys. Res. Lett.*, *24*, 1939–1942.

Meerkötter, R., J. Verdebout, L. Bugliaro, K. Edvardsen, and G. Hansen (2003), An evaluation of cloud affected UV radiation from polar orbiting and geostationary satellites at high latitudes, *Geophys. Res. Lett.*, *30*(18), 1956, doi:10.1029/2003GL017850.

Mims, F. M., and J. E. Frederick (1994), Cumulus clouds and UV-B, *Nature*, *371*, 291.

Nack, M. L., and A. E. S. Green (1974), Influence of clouds, haze, and smog on the middle ultraviolet reaching the ground, *Appl. Opt.*, *13*, 2405–2415.

Peeters, P. K., J.-F. Müller, P. C. Simon, E. Celarier, and J. Herman (1998), Estimation of UV flux at the Earth's surface using GOME data, *Earth Obs. Q.*, *58*, 39–40.

Scheirer, R., and A. Macke (2001), On the accuracy of the independent column approximation in calculating downward fluxes in the UVA, UVB, and PAR spectral ranges, *J. Geophys. Res.*, *106*, 14,301–14,312.

Slaper, H., J. Matthijsen, P. N. den Outer, and G. J. M. Velders (2001), Climatology of Ultraviolet Budgets Using Earth Observation (CUBEO): Mapping UV from the perspective of risk assessments, *BCRS USP-2 Proj. 4.1/AP-03, Rep. 00-17*, Neth. Remote Sens. Board, Delft, Netherlands.

Varnai, T., and A. Marshak (2001), Statistical analysis of the uncertainties in cloud optical depth retrievals caused by three-dimensional radiative effects, *J. Atmos. Sci.*, *58*, 1540–1548.

Verdebout, J. (2000), A method to generate surface UV radiation maps over Europe using GOME, Meteosat, and ancillary geophysical data, *J. Geophys. Res.*, *105*, 5049–5058.

Verdebout, J., and P. Vogt (2002), Satellite-derived UV maps over Europe: Method and applications, in *Ultraviolet Ground- and Space-Based Measurements, Models, and Effects*, *SPIE Proc. Ser.*, vol. 4482, pp. 240–248, SPIE, Bellingham, Wash.

World Meteorological Organization (1986), A preliminary cloudless standard atmosphere for radiation computation, *World Clim. Res. Progr. WMO/TD-24*, Geneva.

Wuttke, S., J. Verdebout, and G. Seckmeyer (2003), An improved algorithm for satellite-derived UV radiation, *Photochem. Photobiol.*, *77*, 107–112.

Zinner, T. (2004), Fernerkundung inhomogener Bewölkung und deren Einfluss auf die solare Strahlungsbilanz, PhD. thesis, Ludwig-Maximilians-Univ., Munich, Germany.

L. Bugliaro, B. Mayer, and R. Meerkötter, Institute for Atmospheric Physics, DLR Oberpfaffenhofen, D-82234 Wessling, Germany. (luca.bugliaro@dlr.de; bernhard.mayer@dlr.de; ralf.meerkoetter@dlr.de)

J. Verdebout, European Commission-Joint Research Centre, Institute for Health and Consumer Protection, Via E. Fermi, I-21020 Ispra, Italy. (jean.verdebout@jrc.it)